

Communication

# Manipulation of the Martensitic Transformation and Exchange Bias Effect in the Ni<sub>45</sub>Co<sub>5</sub>Mn<sub>37</sub>In<sub>13</sub> Ferromagnetic Shape Memory Alloy Films

Jiahong Wen<sup>1,2</sup>, Bochu Yang<sup>1</sup>, Zhichao Dong<sup>3</sup> , Yaxin Yan<sup>1</sup> and Xiaoyu Zhao<sup>3,\*</sup><sup>1</sup> The College of Electronics and Information, Hangzhou Dianzi University, Hangzhou 310018, China<sup>2</sup> Shangyu Institute of Science and Engineering, Hangzhou Dianzi University, Shaoxing 312000, China<sup>3</sup> College of Materials and Environmental Engineering, Hangzhou Dianzi University, Hangzhou 310018, China

\* Correspondence: zhaoxy@hdu.edu.cn

**Abstract:** The martensitic phase transition and exchange bias effect of the Ni-Mn-based ferromagnetic shape memory alloys (FSMAs) Ni<sub>45</sub>Co<sub>5</sub>Mn<sub>37</sub>In<sub>13</sub> (Ni-Co-Mn-In) films are investigated in this paper. The martensitic transformation properties of the Ni-Co-Mn-In alloy target material are manipulated by the process of electric arc melting, melt-fast quenching, and high-temperature thermal pressure. The Ni-Co-Mn-In alloy films with martensite phase transition characteristics are obtained by adjusting deposition parameters on the (001) MgO substrate, which shows a significant exchange bias (EB) effect at different temperatures. With increasing sputtering power and time, the film thickness increases, resulting in a gradual relaxation of the constraints at the interface between the film and the substrate (the interfacial strain decreases as the increase of thin film thickness), which promotes the martensite phase transition. Between zero-field cooling (ZFC) and field-cooled (FC) curve obvious division zone, the decrease of exchange bias field (H<sub>EB</sub>) and coercive force field (H<sub>c</sub>) with an increase in test temperature is due to ferromagnetic (FM) interaction begins to dominate, resulting in a reduction of antiferromagnetic (AFM) anisotropy at the interface. The maximal H<sub>EB</sub> and H<sub>c</sub> reach ~465.7 Oe and ~306.9 Oe at 5 K, respectively. The manipulation of the martensitic transformation and EB effect of the Ni-Co-Mn-In alloy films demonstrates potential application in the field of information and spintronics.

**Keywords:** ferromagnetic shape memory alloys; magnetic phase change Ni-Co-Mn-In alloy film; exchange bias effect



**Citation:** Wen, J.; Yang, B.; Dong, Z.; Yan, Y.; Zhao, X. Manipulation of the Martensitic Transformation and Exchange Bias Effect in the Ni<sub>45</sub>Co<sub>5</sub>Mn<sub>37</sub>In<sub>13</sub> Ferromagnetic Shape Memory Alloy Films. *Magnetochemistry* **2023**, *9*, 51. <https://doi.org/10.3390/magnetochemistry9020051>

Academic Editor: Shengcan Ma

Received: 14 October 2022

Revised: 6 February 2023

Accepted: 6 February 2023

Published: 8 February 2023



**Copyright:** © 2023 by the authors. Licensee MDPI, Basel, Switzerland. This article is an open access article distributed under the terms and conditions of the Creative Commons Attribution (CC BY) license (<https://creativecommons.org/licenses/by/4.0/>).

## 1. Introduction

The NiMn-based ferromagnetic shape memory alloys (FSMAs) with first-order magnetic phase transition are a multifunctional material and have been intensively investigated both experimentally and theoretically, such as magnetocaloric effect (MCE), barocaloric effect (BCE), exchange bias (EB) effect, which have shown potential applications in the microactuator, magnetic sensor, magnetic refrigeration and so on [1–5]. The NiMn-based FSMAs can be induced by both magnetic and temperature fields to achieve the magnetic phase transition between martensite and austenite. And the magnetization and lattice constants of FSMAs can occur mutation near the phase transition temperature. The representative FSMAs material is the Ni<sub>2</sub>MnGa alloy [6]. Where after, new Ni-Mn-based FSMAs are observed such as Ni-Mn-X (X = In, Sn, Sb, and so on) alloys [7]. Among them, the Co doping Ni-Mn-based FSMAs have attracted widespread attention and are systematically studied. For example, the Co doping Ni-Mn-X alloys are highly sensitive to their magneto-structural behavior to micro-structural changes [8]. Wang et al. investigated the manipulation of electric field on MCE in a Ni<sub>44</sub>Co<sub>5.2</sub>Mn<sub>36.7</sub>In<sub>14.1</sub> alloy ribbon/(001)0.7Pb(Mg<sub>1/3</sub>Nb<sub>2/3</sub>)O<sub>3</sub>–0.3PbTiO<sub>3</sub>. The thermal and magnetic hysteresis of the FSMAs can be obviously reduced and the operating temperature window of the alloy ribbon can be remarkably extended [9].

In addition, Wang et al. also revealed that the  $\text{Ni}_{49.8}\text{Co}_{1.2}\text{Mn}_{33.5}\text{In}_{15.5}$  bulk has a large inverse MCE with an  $\Delta S_M$  of  $14.6 \text{ J kg}^{-1} \text{ K}^{-1}$  [10]. Porcar, L. et al. show that the martensitic transformation temperature of the  $\text{Ni}_{45}\text{Co}_5\text{Mn}_{50-x}\text{In}_x$  ( $12.5 \leq x \leq 13.2$ ) ribbons are controlled by In content and the ribbons bending strain is up to 1% [11]. Besides, the effects of alloy composition, heat treatments, and order domain coarsening phenomenon on the martensitic transformation have been investigated in different compositions and processing NiCoMnIn FSMAs by Karaman, I. et al. [12]. Furthermore, Fähler, S. et al. revealed that epitaxial  $\text{Ni}_{48}\text{Co}_5\text{Mn}_{35}\text{In}_{12}$  alloy films deposited on a MgO (100) substrate exhibited metamagnetic transitions and an inverse magnetocaloric effect  $\Delta S_M$  of  $8.8 \text{ J kg}^{-1} \text{ K}^{-1}$  at the 9T field [13]. The effect of the in situ annealing temperature on the martensite transformation of the  $\text{Ni}_{50}\text{Mn}_{38}\text{Co}_6\text{In}_6$  alloy film deposited on the  $\text{SiO}_2$  substrate was systematically investigated by Rios, S. et al. [14].

The exchange bias (EB) effect is defined as the shift in the magnetic hysteresis (M-H) loop of the material from the original due to unidirectional anisotropy produced by the coupling of ferromagnetic (FM) to antiferromagnetic (AFM) at the interface, which is a major magnetic coupling effect and has attracted much attention due to its potential applications in the fields of magnetic recording devices, spintronics devices, and so on [15–17]. It is usually characterized by an EB field ( $H_{EB}$ ) and a coercive force field ( $H_c$ ) varying with the temperature or magnetic field. The EB effect has been observed in many systems, such as nanoparticles, bulk alloys, and films, which are strongly dependent on the composition material, thickness, deposition temperature, post-annealing, and external fields [18–20]. For example, the coexistence of ferromagnetic and spin-glass in the bulk  $\text{Ni}_2\text{Mn}_{1.4}\text{Ga}_{0.6}$  alloy at low temperatures is considered the origin of the EB effect [21]. The generation of the EB in the all-3d-metal  $\text{Ni}_{38.8}\text{Co}_{2.9}\text{Mn}_{37.9}\text{Ti}_{20.4}$  alloy film is attributed to the FM clusters and the AFM host exchange interaction at low temperatures. Here, the Ni-Mn-based FSMAs  $\text{Ni}_{45}\text{Co}_5\text{Mn}_{37}\text{In}_{13}$  (Ni-Co-Mn-In) alloy target material is manipulated by the process of electric arc melting, melt-fast quenching, and high-temperature thermal pressure. The Ni-Co-Mn-In films are deposited on a (100) MgO substrate by sputtering the target material, which shows martensite phase transition characteristics and significant EB effect at different temperatures. The maximal  $H_{EB}$  and  $H_c$  reach  $\sim 465.7 \text{ Oe}$  and  $\sim 306.9 \text{ Oe}$  at 5 K, respectively. The manipulation of the martensitic transformation and EB effect of the Ni-Co-Mn-In alloy film demonstrates potential application in the field of information and spintronics.

## 2. Experiment Details

### 2.1. Preparation of Ni-Co-Mn-In Alloy Target Material

Figure 1 shows the process of making the Ni-Co-Mn-In alloy target material was combined by the electric arc melting, melt-fast quenching, and high-temperature thermal pressure (powder metallurgy method). First, the raw materials were at a purity of 99.99 wt.%-Ni, 99.97 wt.%-Co, 99.95 wt.%-Mn, 99.99 wt.%-In, respectively. The introduction of Co to replace Ni can enhance the magnetization and regulate the phase transition temperature. The Ni-Co-Mn-In alloy ingot was prepared by arc melting method, and the Mn-Co-Mn ferromagnetic moment was formed by adding the Co element to cast the multi-combination alloy ingot (Figure 1a). The process of casting the ingot improves the purity and density of the alloy to enable sufficient alloying of these elements. Secondly, the Ni-Co-Mn-In alloy magnetic phase transition alloy thin ribbons with a length of 1–15 cm and 20–50  $\mu\text{m}$  thick were successfully prepared at different wheel speeds (Figure 1b). The crystal structure of Ni-Co-Mn-In alloy thin ribbons was characterized by using X-ray diffraction (XRD, Smart lab 9 kW, RIGAKU, Tokyo, Japan) at room temperature (RT). Thirdly, the ribbons were ground into an alloy powder under the condition of air isolation and easy heat dissipation. The granularity of the alloy powder prepared was 90–150 mash. After grinding the alloy powder, it was placed at room temperature and air-dried for 0.5 to 2 h (Figure 1c). In addition, the Ni-Co-Mn-In alloy powder with magnetic phase transition was obtained through the fine-tuning of the alloy ingot element content, mixed in a certain proportion, and then imported into the mortar to continue grinding in the

environment of absolute ethanol, to ensure the granularity and mixing uniformity of the alloy mixing powder. Finally, the four-element alloy Ni-Co-Mn-In alloy target material was prepared by high-temperature thermal pressure (powder metallurgy). The prepared alloy mixing powder was installed in the sintering mold, and the mold into the sintering furnace. Vacuuming into the protective gas (nitrogen, argon, etc.) atmosphere, the gas pressure was 1 atm. During thermal pressure, the furnace background vacuum was  $\leq 3 \times 10^{-2}$  Pa, heating the furnace to 600–900 °C (heating rate 6 °C/min) at 20–40 MPa pressure. After thermal insulation and pressure preservation for a certain time (3 h), the pressure was unloaded to the pressure-free room temperature condition, and the finished Ni-Co-Mn-In alloy target material was made after grinding and external round grinding (Figure 1d).

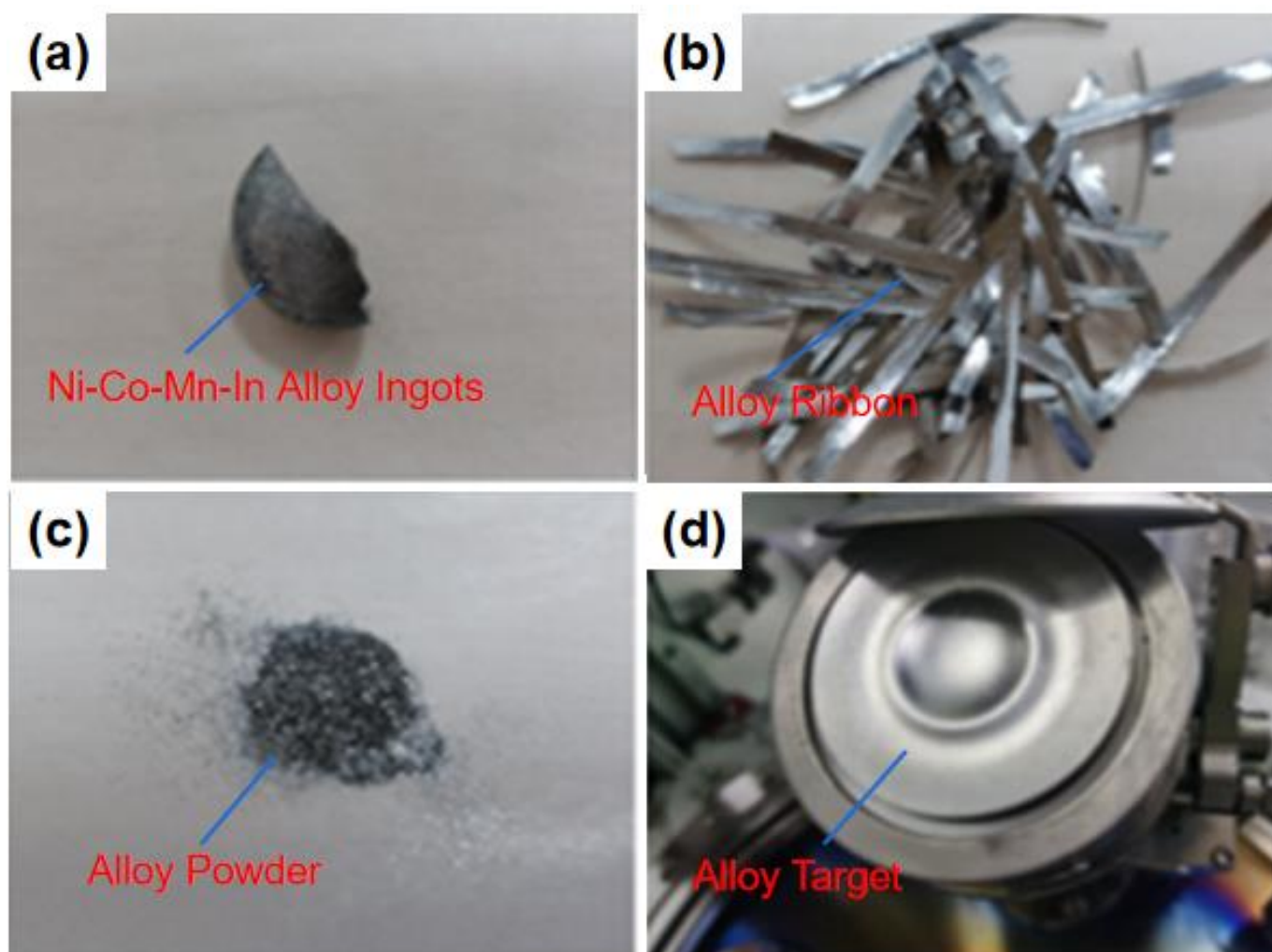


**Figure 1.** The preparation process of the Ni-Co-Mn-In magnetic phase transition alloy target material. (a) The Ni-Co-Mn-In alloy ingots by arc melting. (b) The Ni-Co-Mn-In alloy thin ribbon by melt spinning. (c) The Ni-Co-Mn-In alloy thin ribbon grind to the alloy powder. (d) The hot briquetting Ni-Co-Mn-In alloy target material by high temperature and pressure.

## 2.2. Preparation of Ni-Co-Mn-In Alloy Films

Schematic fabrication of the Ni-Co-Mn-In alloy films was shown in Figure 2a–d. The Ni-Co-Mn-In films were deposited on a (001) MgO substrate in 5 mm × 5 mm × 0.5 mm by the direct current (DC) magnetron sputtering system. During deposition, the target spacing was 10 cm and the substrate was circumgyrated at 10 rpm to achieve a uniform thickness and uniformity. After deposition, the films were annealed in situ for 30 min at 750 °C to improve the crystallinity and structural ordering. A table including the obtention

parameters of each of the Ni-Co-Mn-In alloy films is shown in Table 1. The microstructure and surface topography of the Ni-Co-Mn-In alloy films were determined by the scanning electron microscopy (SEM, JSM-IT300HR, JEOL, Tokyo, Japan) equipped with energy dispersive spectroscopy (EDS) and the Atomic Force Microscope (AFM, 4-NanoScience, JPK, Shanghai, China). The phase transition temperature and magnetic properties of the Ni-Co-Mn-In alloy films were investigated using a superconducting quantum interference device magnetometer (SQUID, MPMS3, Quantum Design, San Diego, CA, USA).

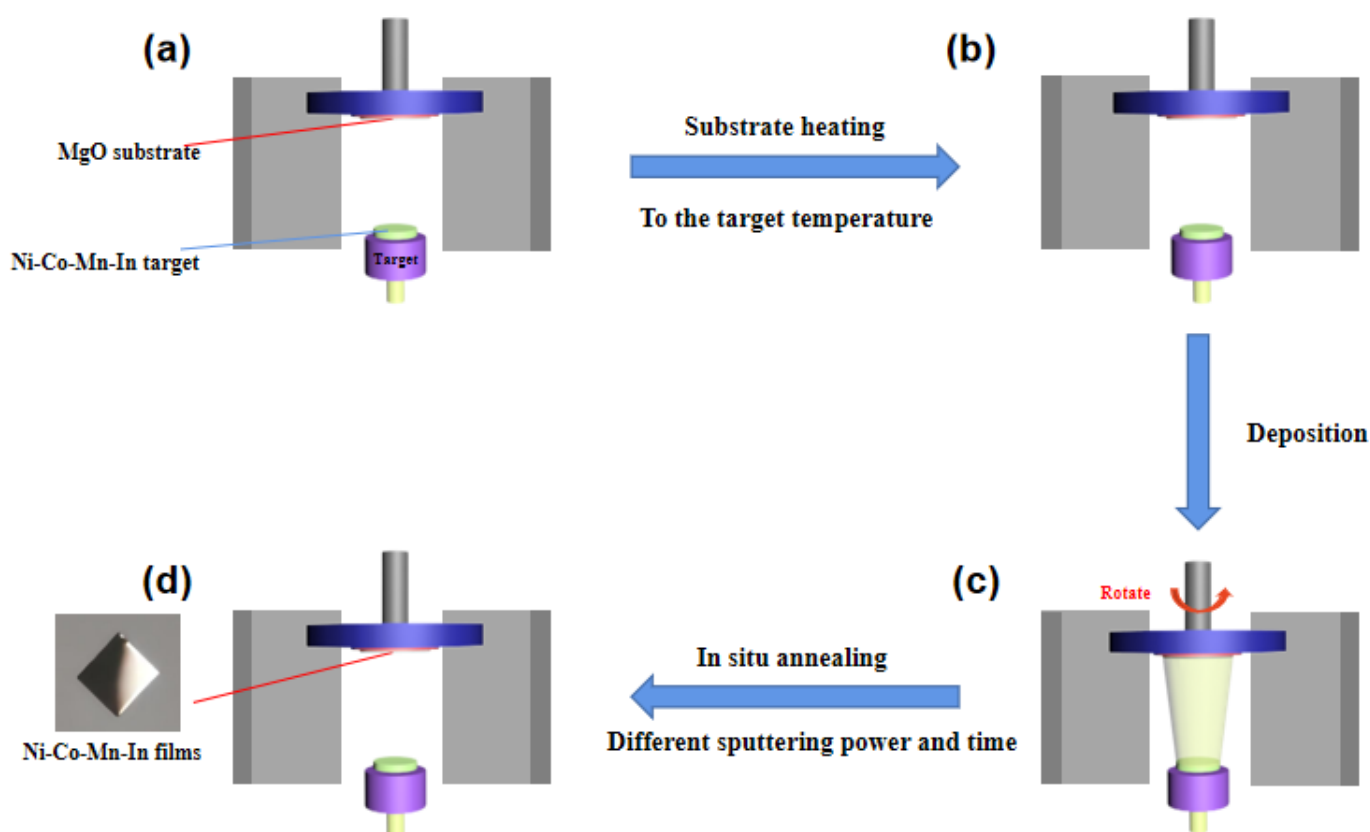


**Figure 2.** Schematic fabrication of the Ni-Co-Mn-In alloy thin film. (a) Put in the substrate; (b) Heater the sample table; (c) Deposition; (d) Annealing.

**Table 1.** The obtention parameters of each sample for the Ni-Co-Mn-In alloy films.

Samples	Power (W)	Time (min)	Temperature (°C)
#1	30	30	750
#2	75	30	750
#3	100	30	750
#4	75	40	750

### 3. Results and Discussion

Figure 3 shows the morphology, crystal structure, and magnetic characterization of the Ni-Co-Mn-In alloy thin ribbons at different wheel speeds (10 m/s, 15 m/s, 25 m/s). The SEM images of the thin ribbons cross-section of the Ni-Co-Mn-In alloy at different wheel speeds are shown in Figure 3a–c, respectively. We can observe the cylindrical particles inside the Ni-Co-Mn-In alloy thin ribbons growing regularly perpendicular to the free surface. With the increasing wheel speed, the cross-sectional thickness of the Ni-Co-Mn-In alloy thin ribbons decreases, approximately reaching 47.5  $\mu\text{m}$  (10 m/s), 37.4  $\mu\text{m}$  (15 m/s), and 19.1  $\mu\text{m}$  (25 m/s), respectively. Figure 3d is the XRD curves of

the Ni-Co-Mn-In alloy thin ribbons at different wheel speeds, which show the crystal structure of the Ni-Co-Mn-In is the austenite phase and the martensite phase transition temperature is around room temperature. As the wheel speed increases, the austenitic phase ratio gradually increases, which indicates the martensite phase transition temperature is gradually moving towards low temperature [4]. The thermomagnetic (M-T) curves of the Ni-Co-Mn-In alloy thin ribbons at different wheel speeds indicate the reverse martensite and martensite phase transition, which is shown in Figure 3e. The thermal lag ( $\Delta T_{hys}$ ) generated by the phase transition process can be calculated as  $T_A - T_M$  using the maximum value on the  $dM/dT$  vs.  $T$  curve for the heating ( $T_A$ ) and cooling ( $T_M$ ) processes (Figure 3f). The corresponding  $T_A$  ( $T_M$ ) is 316.22 K (286.44 K), 310.02 K (272.17 K), and 287.99 K (223.97 K) at different wheel speeds, respectively. The magnetization difference ( $\Delta M$ ) and  $\Delta T_{hys}$  of the Ni-Co-Mn-In alloy thin ribbons at different wheel speeds: the  $\Delta M$  is about 61.4 emu/g (10 m/s), 78.7 emu/g (15 m/s), and 81.5 emu/g (25 m/s); The  $\Delta T_{hys}$  is approximately 29.78 K (10 m/s), 37.85 K (15 m/s), and 64.02 K (25 m/s), respectively. With the increasing wheel speed, the average grain size, unit cell volume, martensitic transformation temperature, and magnetic parameters of the thin ribbon decrease, which increases the defect density, leading to the phase transition temperature of the Ni-Co-Mn-In alloy thin ribbons gradually moving towards the low temperature [22]. The characterization of the Ni-Co-Mn-In alloy thin ribbons is essential for the preparation of the alloy target material, which determines the structural and magnetic properties of the Ni-Co-Mn-In alloy targets and films.

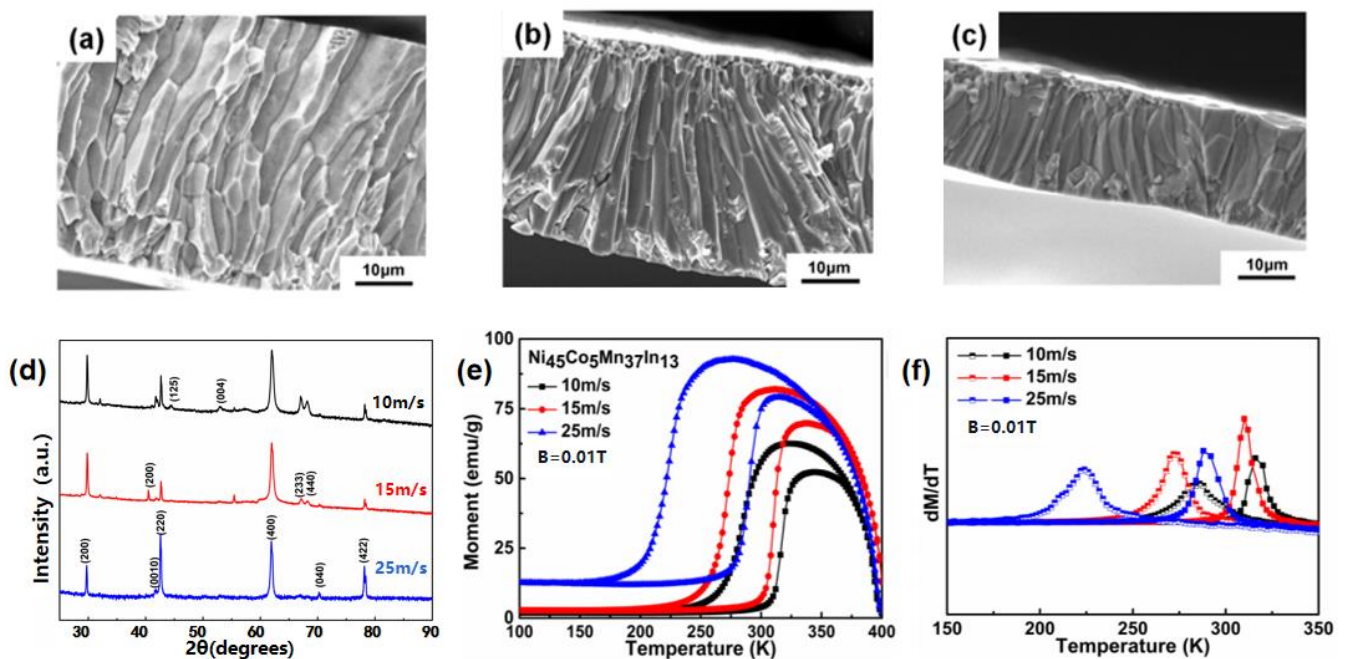


**Figure 3.** The morphology, crystal structure, and magnetic characterization of the Ni-Co-Mn-In alloy thin ribbons with different wheel speeds (10 m/s, 15 m/s, 25 m/s). SEM (a–c), XRD (d), M-T (e) and  $dM/dT$  (f).

Figure 4 shows the surface morphology and composition uniformity of the Ni-Co-Mn-In alloy films (with different sputtering power and time (#1–#4) as shown in Table 1). The grain size increases with the sputtering power increase as shown in Figure 4a–c. With increasing power (#1–#3), the energy acquired by the plasma increases, leading to smaller particles, the ion bombardment strength of the target surface, and the number of atoms sputtered out increasing. Smaller particles have higher surface free energy that can aggregate faster and grow into larger particles, eventually growing into irregular island particles [23,24]. With the increasing sputtering time, the crystallization of the

sample (#4) increases, making the particle size reduced and almost evenly distributed (Figure 4d). Combined with the EDS mapping images, the element of the Ni-Co-Mn-In alloy films are relatively evenly distributed as shown in Figure 4(a-i)–(d-i). The surface morphology of films measured by AFM agrees with that measured by SEM, which is shown in Figure 4(a-ii)–(d-ii). The roughness of root mean square  $R_q$  for #1–#4 samples is 10.93 nm, 15.03 nm, 34.52 nm, 10.10 nm, and Average surface roughness  $R_a$  is 8.34 nm, 10.99 nm, 28.86 nm, 7.30 nm, respectively.

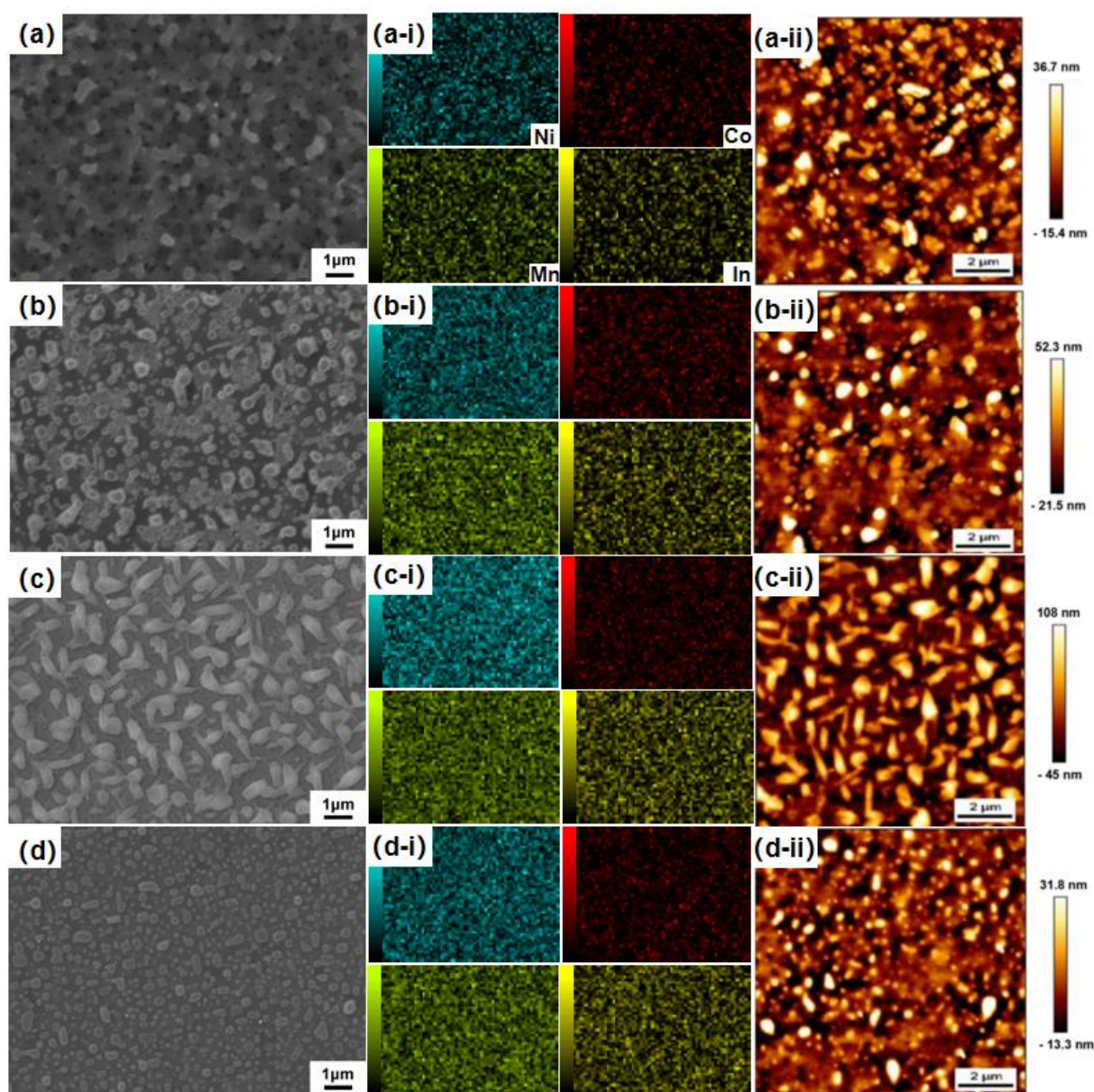


**Figure 4.** The surface morphology of the Ni-Co-Mn-In alloy thin films (samples label #1–#4) is characterized by SEM (a–d) and AFM (a-ii)–(d-ii). The composition uniformity of the Ni-Co-Mn-In alloy thin films (samples label #1–#4) is characterized by EDS (a-i)–(d-i).

The M-T curves of the Ni-Co-Mn-In alloy films (#1–#4) are measured using the SQUID at a magnetic field strength of  $H = 0.01$  T, which are shown in Figure 5. The Ni-Co-Mn-In alloy films are first cooled from 300 K to 100 K without the magnetic field and then the samples are subjected to zero-field cooling (ZFC) curve measurement under the magnetic field heating conditions from 100 K to 400 K. Next, the field-cooled (FC) curve measurement is performed while cooling down the sample in the presence of the magnetic field from

400 K to 100 K. Finally, the samples are warmed in the presence of magnetic field from 100 K to 400 K (FW). The Ni-Co-Mn-In alloy films undergo a phase transition from parent austenite to martensite, which characteristic temperatures include austenite start ( $A_s$ ), finish ( $A_f$ ), martensite start ( $M_s$ ), and finish ( $M_f$ ) temperatures. The ferromagnetic order transition temperature (Curie temperature  $T_c$ ) of the Ni-Co-Mn-In alloy films gradually increases (#1–#4) to 325.89 K, 337.48 K, 338.34 K, and 342.07 K, respectively. When the sputtering power is 30 W and the time is 30 min, no phase transition occurs as shown in Figure 5a. The absence of phase transformation in the Ni-Co-Mn-In alloy film (#1) is due to a mismatched lattice between the substrate and the film, leading to internal strain that causes lattice distortion. In addition, the small grain size brings a large number of boundaries acting as barriers separating the individual grains, which provide a transformation energy barrier and restrict the growth of the martensite phase. With the increase of sputtering power and time (the increase of film thickness), the strain imposed by both the alloy film and MgO substrate interface reduces (strain relaxation), which promotes grain size growth. With the grain size increases, the grain boundaries and the width of the intergranular region decreases which in turn decreases the energy barrier which is responsible to restrict the martensitic transformation [23,24]. Besides, the increase in grain size leads to a reduction in strain energy, and thus less driving force is required for transformation, which facilitates from the slight signature of phase transition to a significant phase transition (Figure 5b–d).

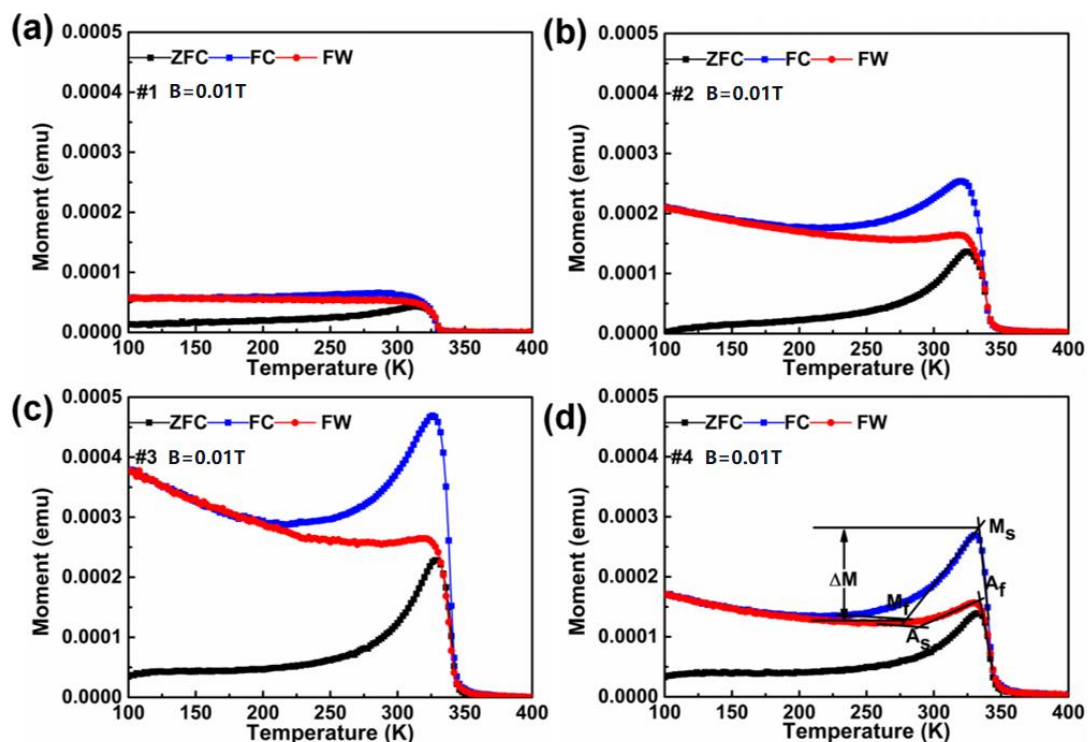


**Figure 5.** The M-T curves with ZFC, FC, and FW measurement for the Ni-Co-Mn-In alloy films. (a) #1, (b) #2, (c) #3, (d) #4.

The EB effect of the Ni-Co-Mn-In alloy film (#3) with prominent and well-defined martensitic transformation is shown by the magnetic hysteresis loops (M-H) curves at different temperatures in the applied field  $\pm 2000$  Oe (Figure 6a,b). With decreasing the test temperature, the M-H shifts towards the negative field axis and shows a significant EB effect on the Ni-Co-Mn-In alloy film. In the  $0 \rightarrow (+H) \rightarrow 0 \rightarrow (-H)$  period, M-H exhibits a shift towards the negative field axis. In the  $(-H) \rightarrow 0 \rightarrow (+H)$  period, M-H shows a shift towards the positive field axis. Both periods as shown in the partially enlarged drawing Figure 6b. The presence of the EB effect in the Ni-Co-Mn-In alloy film is due to FM and AFM coupling at the interface (Figure 6c,d) [25]. The coupling between AFM and FM spins

exerts an additional torque on the FM spins. After the films are cooled in the presence of the field, the FM and AFM spins become parallel to each other at the interface. When the field direction is reversed, the FM spins start rotating but the AFM spins remain fixed if the AFM anisotropy is large enough to get affected by the reversibility of field direction. Consequently, the AFM spins exert torque on the FM spins to keep them in their original position. Thus, the magnetic field required to completely reverse the magnetization in the FM is higher when it is coupled to AFM as compared to the uncoupled FM because an extra field is required to overcome the torque exerted by AFM spins. Conversely, when the magnetic field is again reversed back, the rotation of FM spins is easier than in an uncoupled FM since the AFM spins now favor the magnetization reversal as they now exert torque in the direction of the applied magnetic field. Owing to this unidirectional anisotropy, the hysteresis loops get shifted along the field axis resulting in EB behavior [26]. The  $H_{EB}$  and  $H_C$  are defined as  $H_{EB} = -(H_L + H_R)/2$  and  $H_C = |H_L - H_R|/2$ , where  $H_L$  is the left branch coercivity and  $H_R$  is the right branch coercivity, respectively. For the Ni-Co-Mn-In alloy film (#3), the maximal  $H_{EB}$  and  $H_C$  are about  $\sim 466$  Oe and  $\sim 307$  Oe at 5 K, respectively. The  $H_{EB}$  and  $H_C$  decrease with increasing temperature, which is shown in Table 2. Besides, the smaller degree of exchange bias effect exists around 300 K and the absolute value of  $H_{EB}$  is almost constant above 300 K.

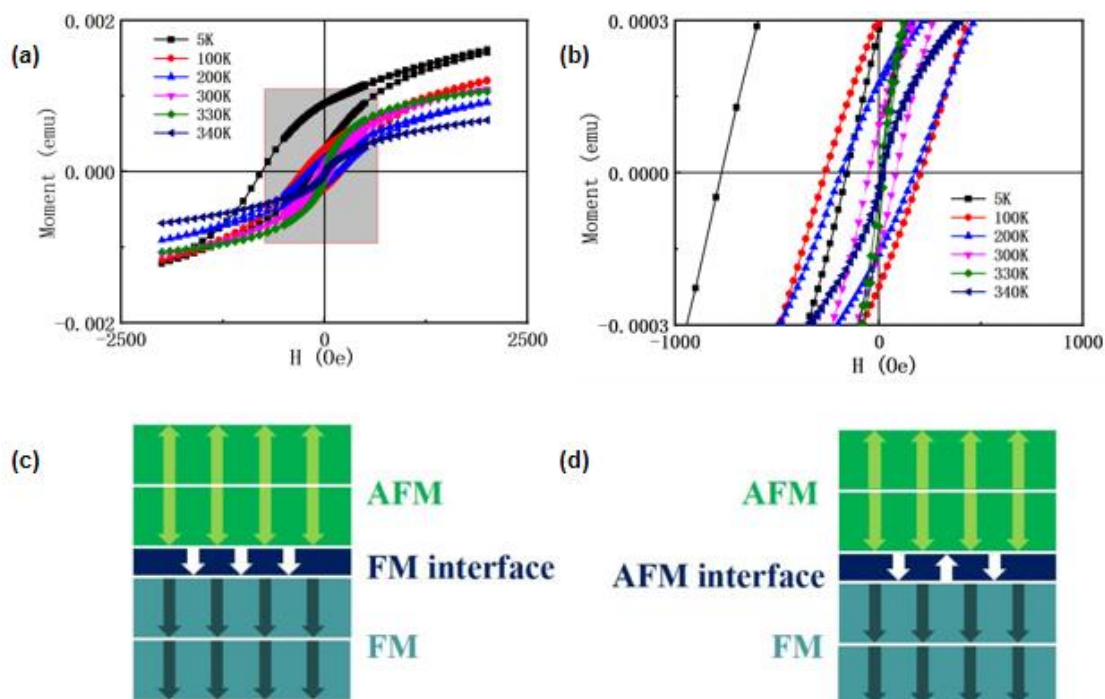


**Figure 6.** The M-H curves of the Ni-Co-Mn-In alloy film (#3) at different temperatures (a,b). The schematic diagram for the EB effect (c,d).

**Table 2.** The  $H_L$ ,  $H_R$ ,  $H_{EB}$ , and  $H_C$  for the Ni-Co-Mn-In alloy film (#3) at different temperatures.

Temperature (K)	$H_L$ (Oe)	$H_R$ (Oe)	$H_{EB} = -(H_L + H_R)/2$ (Oe)	$H_C =  H_L - H_R /2$ (Oe)
5 K	-772.6	-158.8	465.7	306.9
100 K	-263.8	205.0	29.4	234.4
200 K	-185.2	175.5	4.9	180.4
300 K	-49.0	83.9	-17.5	66.5
330 K	7.8	27.4	-17.6	9.8
340 K	12.9	22.1	-17.5	4.6

#### 4. Conclusions

In this article, we study the effects of different preparation parameters on the martensitic transformation and EB effect for the Ni-Mn-based FSMAs Ni<sub>45</sub>Co<sub>5</sub>Mn<sub>37</sub>In<sub>13</sub> (Ni-Co-Mn-In) films. With increasing sputtering power and time, the film thickness increases, resulting in a gradual relaxation of the constraints at the interface between the film and the substrate and changing the interfacial stress, promoting the growth of particle size and the martensite phase transition. More importantly, the Ni-Co-Mn-In alloy films have a significant EB effect at different temperatures, which is related to the mutual coupling strength of FE to AFM. The manipulation of the martensitic transformation and EB effect for the Ni-Co-Mn-In alloy films demonstrate potential application in the field of information and spintronics.

**Author Contributions:** J.W. and B.Y. contributed equally to this work. J.W.: Conceptualization, Funding acquisition, Writing—review & editing. B.Y.: Data curation, Investigation, Methodology. Z.D. and Y.Y.: Investigation, Methodology, Data curation, Writing—original draft. X.Z.: Funding acquisition, Writing—review & editing. All authors have read and agreed to the published version of the manuscript.

**Funding:** This work is supported by the National Natural Science Foundation of China (Nos. 51901060, 12004090); the National Natural Science Foundation of Zhejiang Province (Nos. LY21E010004, LQ21A040009); the Fundamental Research Funds for the Provincial Universities of Zhejiang (No. GK209907299001-025).

**Institutional Review Board Statement:** Not applicable.

**Informed Consent Statement:** Not applicable.

**Data Availability Statement:** Not applicable.

**Conflicts of Interest:** The authors declare no conflict of interest.

#### References

1. Wei, Z.Y.; Shen, Y.; Zhang, Z.; Guo, J.P.; Li, B.; Liu, E.; Zhang, Z.D.; Liu, J. Low-pressure induced giant barocaloric effect in an all-d-metal Heusler Ni<sub>35.5</sub>Co<sub>14.5</sub>Mn<sub>35</sub>Ti<sub>15</sub> magnetic shape memory alloy. *APL Mater.* **2020**, *8*, 051101. [[CrossRef](#)]
2. Yang, Q.; Zhou, Z.; Sun, N.; Liu, M. Perspectives of voltage control for magnetic exchange bias in multiferroic heterostructures. *Phys. Lett. A* **2017**, *381*, 1213–1222. [[CrossRef](#)]
3. Zhao, X.; Yan, Y.; Wen, J.; Li, Y.; Li, L. Enhancement of magnetocaloric effect in all-d-metal Heusler Mn<sub>52.6</sub>Ni<sub>30.5</sub>Co<sub>7.8</sub>Ti<sub>9.1</sub>/PVA/PET flexible composite by mechanical strains. *J. Alloys Compd.* **2022**, *897*, 163116. [[CrossRef](#)]
4. Zhao, X.; Wen, J.; Gong, Y.Y.; Ma, S.C.; Hu, Q.B.; Wang, D.H. Nonvolatile manipulation of the magnetocaloric effect in Ni<sub>43</sub>Co<sub>7</sub>Mn<sub>39</sub>Sn<sub>11</sub>/(011)PMN-PT composite by electric fields. *Scripta Mater.* **2019**, *167*, 41–45. [[CrossRef](#)]
5. Chen, J.; Tu, R.; Fang, X.; Gu, Q.; Zhou, Y.; Cui, R.; Han, Z.; Zhang, L.; Fang, Y.; Qian, B.; et al. Probing the ground state and zero-field cooled exchange bias by magnetoresistance measurement in Mn<sub>50</sub>Ni<sub>41</sub>Sn<sub>9</sub> ribbon. *J. Magn. Magn. Mater.* **2017**, *426*, 708–713. [[CrossRef](#)]
6. Karim, A.; Guan, C.S.; Chen, B.; Li, Y.; Zhang, J.W.; Zhu, L.; Deng, X.; Hu, Y.; Bi, K.Q.; Li, H.L.; et al. Dynamic observation of joule heating-induced structural and domain transformation in smart shape-memory alloy. *Acta Mater.* **2020**, *186*, 223–228. [[CrossRef](#)]
7. Sutou, Y.; Imano, Y.; Koeda, N.; Omori, T.; Kainuma, R.; Ishida, K.; Oikawa, K. Magnetic and martensitic transformations of NiMnX (X = In, Sn, Sb) ferromagnetic shape memory alloys. *Appl. Phys. Lett.* **2004**, *85*, 4358–4360. [[CrossRef](#)]
8. Dubiel, Ł.; Wal, A.; Stefaniuk, I.; Żywczak, A.; Maziarz, W. Electron magnetic resonance study of the Ni<sub>47</sub>Co<sub>3</sub>Mn<sub>35.5</sub>In<sub>14.5</sub> ribbons. *J. Magn. Magn. Mater.* **2021**, *530*, 167930. [[CrossRef](#)]
9. Gong, Y.-Y.; Wang, D.-H.; Cao, Q.-Q.; Liu, E.-K.; Liu, J.; Du, Y.-W. Electric field control of the magnetocaloric effect. *Adv. Mater.* **2015**, *27*, 801–805. [[CrossRef](#)]
10. Huang, L.; Cong, D.Y.; Ma, L.; Nie, Z.H.; Wang, Z.L.; Suo, H.L.; Ren, Y.; Wang, Y.D. Large reversible magnetocaloric effect in a Ni-Co-Mn-In magnetic shape memory alloy. *Appl. Phys. Lett.* **2016**, *108*, 032405. [[CrossRef](#)]
11. Porcar, L.; Miraglia, S.; Porcher, F.; Haettel, R.; Plainedoux, P.; Perticarrari, M.S.; Dufour, H.; Pairis, S.; Jarreau, J.; Verdier, M.; et al. Long flexible melt-spun Ni-Co-Mn-In ribbons with shape memory effect and caloric performances above 300 K. *Materialia* **2019**, *8*, 100493. [[CrossRef](#)]
12. Salas, D.; Wang, Y.; Duong, T.; Attari, V.; Ren, Y.; Chumlyakov, Y.; Arróyave, R.; Karaman, I. Competing Interactions between Mesoscale Length-Scales, Order-Disorder, and Martensitic Transformation in Ferromagnetic Shape Memory Alloys. *Acta Mater.* **2021**, *206*, 116616. [[CrossRef](#)]

13. Niemann, R.; Heczko, O.; Schultz, L.; Fähler, S. Metamagnetic transitions and magnetocaloric effect in epitaxial Ni–Co–Mn–In films. *Appl. Phys. Lett.* **2010**, *97*, 222507. [[CrossRef](#)]
14. Rios, S.; Karaman, I.; Zhang, X. Crystallization and high temperature shape memory behavior of sputter-deposited NiMnCoIn thin films. *Appl. Phys. Lett.* **2010**, *96*, 173102. [[CrossRef](#)]
15. Skumryev, V.; Stoyanov, S.; Zhang, Y.; Hadjipanayis, G.; Givord, D.; Nogues, J. Beating the superparamagnetic limit with exchange bias. *Nature* **2003**, *423*, 850–853. [[CrossRef](#)]
16. Kools, J.C.S. Exchange-biased spin-valves for magnetic storage. *IEEE Trans. Magn.* **1996**, *32*, 3165–3184. [[CrossRef](#)]
17. Matsumoto, H.; Ota, S.; Ando, A.; Chiba, D. A flexible exchange-biased spin valve for sensing strain direction. *Appl. Phys. Lett.* **2019**, *114*, 132401. [[CrossRef](#)]
18. Liu, K.; Ma, S.C.; Zhang, Z.S.; Zhao, X.W.; Yang, B.; Wang, D.H.; Ur Rehman, S.; Zhong, Z.C. Giant exchange bias effect in all-3d-metal Ni<sub>38.8</sub>Co<sub>2.9</sub>Mn<sub>37.9</sub>Ti<sub>20.4</sub> thin film. *Appl. Phys. Lett.* **2020**, *116*, 022412. [[CrossRef](#)]
19. Zhu, C.M.; Wang, L.G.; Liu, F.C.; Kong, W.J. Exchange bias behaviors up to room temperature in NiCo<sub>2</sub>O<sub>4</sub>/NiO nanoparticle system. *Ceram. Int.* **2019**, *45*, 9878–9883. [[CrossRef](#)]
20. Giri, S.; Patra, M.; Majumdar, S. Exchange bias effect in alloys and compounds. *J. Phys.-Condens. Mat.* **2011**, *23*, 073201. [[CrossRef](#)]
21. Han, Z.D.; Qian, B.; Wang, D.H.; Zhang, P.; Jiang, X.F.; Zhang, C.L.; Du, Y.W. Magnetic phase separation and exchange bias in off-stoichiometric Ni–Mn–Ga alloys. *Appl. Phys. Lett.* **2013**, *103*, 172403. [[CrossRef](#)]
22. Ma, C.; Liu, K.; Han, X.; Yang, S.; Ye, N.; Tang, J. Martensitic transformation and magnetocaloric effect in melt-spun Mn<sub>50</sub>Ni<sub>31.5</sub>Co<sub>8.5</sub>Ti<sub>10</sub> all-3d-metal alloy ribbons. *J. Magn. Magn. Mater.* **2020**, *493*, 165733. [[CrossRef](#)]
23. Vishnoi, R.; Kaur, D. Size dependence of martensite transformation temperature in nanostructured Ni–Mn–Sn ferromagnetic shape memory alloy thin films. *Surf. Coat. Technol.* **2010**, *204*, 3773–3782. [[CrossRef](#)]
24. Vishnoi, R.; Singhal, R.; Kaur, D. Thickness dependent phase transformation of magnetron-sputtered Ni–Mn–Sn ferromagnetic shape memory alloy thin films. *J. Nanopart. Res.* **2011**, *13*, 3975–3990. [[CrossRef](#)]
25. Zheng, G.; Xie, W.Q.; Albarakati, S.; Algarni, M.; Tan, C.; Wang, Y.; Peng, J.; Partridge, J.; Farrar, L.; Yi, J.; et al. Gate-tuned interlayer coupling in van der Waals ferromagnet Fe<sub>3</sub>GeTe<sub>2</sub> nanoflakes. *Phys. Rev. Lett.* **2020**, *125*, 047202. [[CrossRef](#)]
26. Akkera, H.S.; Singh, I.; Kaur, D. Martensitic phase transformation of magnetron sputtered nanostructured Ni–Mn–In ferromagnetic shape memory alloy thin films. *J. Alloys Compd.* **2015**, *642*, 53–62. [[CrossRef](#)]

**Disclaimer/Publisher’s Note:** The statements, opinions and data contained in all publications are solely those of the individual author(s) and contributor(s) and not of MDPI and/or the editor(s). MDPI and/or the editor(s) disclaim responsibility for any injury to people or property resulting from any ideas, methods, instructions or products referred to in the content.